tional Suisse is also gratefully acknowledged. We express our appreciation to G. Baudoux and Dr. D. Vercauteren for their help in obtaining the electrostatic potential energy maps.

Registry No. **1**, 107-25-5; **1H$^+$**, 51624-53-4; **2**, 116-11-0; **2H$^+$**, 41798-19-0; **3**, 922-69-0; **3H$^+$**, 81876-12-2; **4**, 1822-74-8; **4H$^+$**, 64840-96-6; **5**, 7594-44-7; **5H$^+$**, 85838-78-4; **6**, 51102-74-0; **6H$^+$**, 105384-19-8; **7**, 76573-19-8; **7H$^+$**, 120991-14-2; **8**, 114659-08-4; **8H$^+$**, 120991-15-3; **9**, 99030-02-1; **9H$^+$**, 90195-92-9.

Supplementary Material Available: The full set of 3-21G-(*)-optimized geometrical parameters for compounds **1-9** and **1H$^+$-9H$^+$** (4 pages). Ordering information is given on any current masthead page.

Production of Hydrated Metal Ions by Fast Ion or Atom Beam Sputtering. Collision-Induced Dissociation and Successive Hydration Energies of Gaseous Cu^+ with 1-4 Water Molecules[1]

Thomas F. Magnera,* Donald E. David,* Dusan Stulik, Robert G. Orth, Harry T. Jonkman, and Josef Michl*

Contribution from the Center for Structure and Reactivity, Department of Chemistry, The University of Texas at Austin, Austin, Texas 78712-1167. *Received September 8, 1988*

Abstract: Low-temperature sputtering of frozen aqueous solutions of metal salts, of hydrated crystalline transition-metal salts, of frosted metal surfaces, and of frosted metal salts with kiloelectronvolt energy rare gas atoms or ions produces copious amounts of cluster ions, among which $M^+(H_2O)_n$ and/or $M^+OH(H_2O)_n$ frequently dominate. Variable-energy collision-induced dissociation of these ions in a triple quadrupole mass spectrometer yields the successive gas-phase solvation energies. Several known hydration and bond energies have been reproduced, and the first and second hydration energies of the Cu^+ ion have been determined as 35 ± 3 and 39 ± 3 kcal/mol, respectively. It is concluded that gaseous Cu^+ prefers dicoordination.

In recent years many ligand-metal ion bond dissociation energies and enthalpies have been measured by thermodynamic equilibrium,[2-4] ion beam,[5,6] FT-ICR collision-induced dissociation,[7] and photodissociation methods.[8] However, reported energies of weak inorganic ligand-metal ion bonds remain relatively scarce and are limited to the hydrates[2] and ammoniates[3a] of alkali-metal cations and their complexes with sulfur dioxide,[3b,4a] hydrates of Ca^+,[3c] Sr^+,[3d] and Pb^+,[3f] and some of the hydrates and ammoniates of Bi^+,[3a,3e] Cu^+, and Ag^+.[4] These ligated metal cations were generated by thermionic metal ion sources[4c] in high-pressure mass spectrometers. Recently, sputtered ions have been used in place of the thermionic metal ion sources in high-pressure mass spectrometers under conditions suitable for making weak ligand-metal ion complexes.[9] For applications where a continuous metal ion source is not necessary, other techniques, notably pulsed laser desorption and ionization,[10,11] produce a wide variety of metal ions and metal clusters.

In the present paper, we describe the use of fast atom or fast ion bombardment of selected substrates for the production of copious amounts of hydrated and/or hydroxylated transition-metal ions and cluster ions. The use of these sources is a logical extension of prior reports of large cluster ion formation upon ion bombardment of frozen ammonia[12] and water,[12,13] as well as other

(1) Much of the work was performed in the Chemistry Department of the University of Utah in Salt Lake City, UT. The results were reported in part at: *Book of Abstracts*; 30th ASMS Annual Conference, Honolulu, June 1982; p 695. 191st National Meeting of the American Chemical Society: New York, NY, April 13-18, 1986; American Chemical Society: Washington, DC, Abstract No. PHYS 93.

(2) Džidič, I.; Kebarle, P. *J. Phys. Chem.* **1970**, *74*, 1466.

(3) (a) Castleman, A. W., Jr. *Chem. Phys. Lett.* **1978**, *53*, 560. Castleman, A. W., Jr.; Holland, P. M.; Lindsay, D. M.; Peterson, K. I. *J. Am. Chem. Soc.* **1978**, *100*, 6039. (b) Tang, I. N.; Munkelwitz, H. R.; Castleman, A. W., Jr. *Nature* **1971**, *230*, 175. (c) Kochanski, E.; Constantin, E. *J. Chem. Phys.* **1987**, *87*, 1661. (d) Tang, I. N.; Lian, M. S.; Castleman, A. W., Jr. *J. Chem. Phys.* **1976**, *65*, 4022. (e) Tang, I. N.; Castleman, A. W., Jr. *J. Chem. Phys.* **1974**, *60*, 3981. (f) Tang, I. N.; Castleman, A. W., Jr. *J. Chem. Phys.* **1972**, *57*, 3638.

(4) (a) Peterson, K. I.; Holland, P. M.; Keesee, R. G.; Lee, N.; Märk, T. D.; Castleman, A. W., Jr. *Surf. Sci.* **1981**, *106*, 136. (b) Holland, P. M.; Castleman, A. W., Jr. *J. Chem. Phys.* **1982**, *76*, 4195. (c) Holland, P. M.; Castleman, A. W., Jr. *J. Am. Chem. Soc.* **1980**, *102*, 6174.

(5) (a) Kang, H.; Beauchamp, J. L. *J. Am. Chem. Soc.* **1986**, *108*, 7502. (b) Halle, L. F.; Armentrout, P. B.; Beauchamp, J. L. *J. Am. Chem. Soc.* **1981**, *103*, 962. (c) Armentrout, P. B.; Halle, L. F.; Beauchamp, J. L. *J. Am. Chem. Soc.* **1981**, *103*, 6501. (d) Armentrout, P. B.; Halle, L. F.; Beauchamp, J. L. *J. Am. Chem. Soc.* **1981**, *103*, 6628. (f) Armentrout, P. B.; Beauchamp, J. L. *J. Chem. Phys.* **1981**, *74*, 2819. (g) Halle, L. F.; Armentrout, P. B.; Beauchamp, J. L. *Organometallics* **1982**, *1*, 963.

(6) (a) Ervin, K. M.; Armentrout, P. B. *J. Chem. Phys.* **1985**, *83*, 166. (b) Aristov, N.; Armentrout, P. B. *J. Am. Chem. Soc.* **1986**, *108*, 1806. (c) Ervin, K.; Loh, S. K.; Aristov, N.; Armentrout, P. B. *J. Phys. Chem.* **1983**, *87*, 3593. (d) For a recent example, see: Schultz, R. H.; Elkind, J. L.; Armentrout, P. B. *J. Am. Chem. Soc.* **1988**, *110*, 411.

(7) Burnier, R. C.; Cody, R. B.; Freiser, B. S. *J. Am. Chem. Soc.* **1982**, *104*, 7436.

(8) Cassady, C. J.; Freiser, B. S. *J. Am. Chem. Soc.* **1984**, *106*, 6176.

(9) Freas, R. B.; Campana, J. E. *J. Am. Chem. Soc.* **1985**, *107*, 6202. Freas, R. B.; Dunlap, B. I.; Waite, B. A.; Campana, J. E. *J. Chem. Phys.* **1987**, *86*, 1276.

(10) Burnier, R. C.; Carlin, T. J.; Reents, W. D., Jr.; Cody, R. B.; Lengel, R. K.; Freiser, B. S. *J. Am. Chem. Soc.* **1979**, *101*, 7127.

(11) Jones, R. W.; Staley, R. H. *J. Am. Chem. Soc.* **1980**, *102*, 3794. Jones, R. W.; Staley, R. H. *J. Am. Chem. Soc.* **1982**, *104*, 2296. Uppal, J. S.; Staley, R. H. *J. Am. Chem. Soc.* **1982**, *104*, 1235. Uppal, J. S.; Staley, R. H. *J. Am. Chem. Soc.* **1982**, *104*, 1238.

(12) Satkiewiez, F. G.; Myer, J. A.; Warneck, P. Techniques Applicable to Mass Spectrometry of Gaseous Trace Contaminants. Interim Report to NASA from the GCA Corp., Bedford, MA, Contract No. NAS 12-G41; 1969.

(13) Lancaster, G. M.; Honda, F.; Fukuda, Y.; Rabalais, J. W. *J. Am. Chem. Soc.* **1979**, *101*, 1951. Lancaster, G. M.; Honda, F.; Fukuda, Y.; Rabalais, J. W. *Int. J. Mass Spectrom. Ion Phys.* **1979**, *29*, 199.

0002-7863/89/1511-5036$01.50/0

materials such as alkali halides,[14] frozen gases,[15] and metals,[16] and of reports of hydrated alkali-metal ion formation by the kiloelectronvolt ion bombardment of alkali halides covered with an adsorbed layer of water.[17]

Variable-energy collision-induced dissociation in a triple quadrupole mass spectrometer was used to measure binding energies of cluster ions generated using this source. Initial experiments revealed that the ejected cluster ions have a broad distribution of internal energies, up to and slightly exceeding the dissociation limit. It is possible to cool the sputtered ions with third-body collisions, but this entails a loss of intensity.[18] We now find that even without cooling it is possible to determine the binding energies with an accuracy of about 10–20%. We have tested the procedure on several cases where the binding energies were already known: the ion series $H_3O^+(H_2O)_n$ (n = 1–4),[19] $Co^+OH(H_2O)$,[8] and $Cr^+OH(H_2O)$.[5a] We have used it to determine the successive hydration energies of H_2O in $Cu^+(H_2O)_n$ (n = 1–4). The values for n = 3–5 were also known previously.[4b]

In our experience, optimal sputtering substrates for the production of hydrated metal ions are (i) frozen aqueous solutions of transition-metal salts, (ii) hydrated crystalline transition-metal salts, (iii) frosted metal surfaces, or (iv) frosted transition-metal salts. In all cases, we keep the substrate cold to prevent the sublimation of ice. The advantage of substrates (i) and (ii) is their essentially unlimited longevity, but the disadvantage is that their surface charges. Substrates (iii) and (iv) can only be used for several hours at 100 $\mu A/cm^2$ primary current density. Substrate (iii) is extremely convenient to use, provides the best signal intensity, and does not suffer from surface charging. A useful modification of methods (iii) and (iv), which provides them with unlimited longevity, is to simultaneously leak water vapor at low pressures into the vacuum chamber, thus continually renewing the frosted substrate. In addition, the thin layer of ice leads to strongly enhanced ion signals from the metal substrate. This is an effect similar to the secondary ion yield enhancement observed when O_2^+ is directed onto the surface.[20] Unfrosted hydrated transition-metal salts (ii) are useful substrates for producing ions of the types M^+OH, $M^+OH(H_2O)$, M_2^+OH, and $M_2^+OH(H_2O)$ but do not produce any extensive hydrated cluster series.

We have also examined the potential that SIMS and FAB of quickly frozen aqueous solutions of inorganic and organic species might have for analytical purposes and for the examination of the degree of ion aggregation in solution.

Experimental Section

Instrumentation. The triple quadrupole instrument is designed for multiple uses, which include FABMS, SIMS, UPS, and laser photodissociation spectroscopy. Since our initial report using this instrument,[21] instruments of similar design have been described.[16]

Commercially available parts were used in the construction whenever possible. The basic elements are three interconnected but separately pumped UHV chambers (Figure 1). The target for the SIMS and UPS experiments is an oxygen-free copper tip attached to either an Air Products Model LT-3-110 Heli-Tran (lowest temperature 2 K) or an Air Products Model CSW-202 closed-cycle cryostat (lowest temperature 12 K). The target can be moved between the preparation chamber and the main chamber by a computer-controlled linear-motion drive. A series of differentially pumped greaseless Teflon seals are used for the motion feedthrough. Gases are deposited onto a cold target through a precision leak valve. This procedure is carried out exclusively in the preparation chamber, which is separated from the rest of the system by a gate valve.

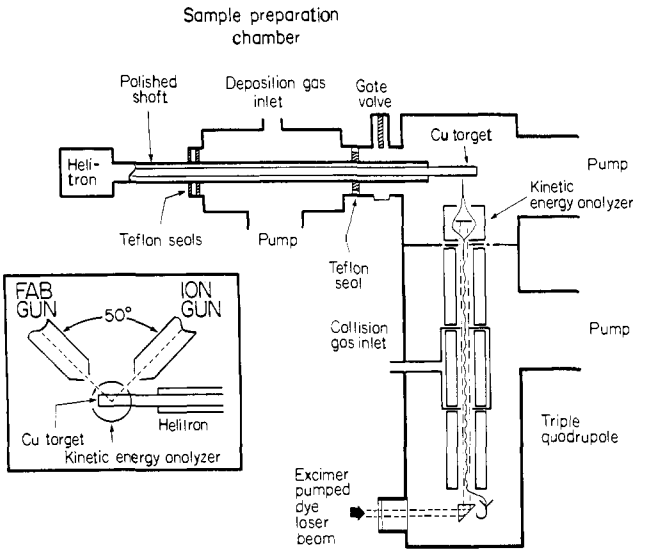

Figure 1. Triple quadrupole secondary ion mass spectrometer.

In the main chamber, the target can be bombarded either by 1–5-keV rare gas ions, produced in a Riber Model CI-50R ion gun, or by 2–10-keV rare gas fast atoms, produced in an Ion Tec Model FAB11NF saddle-field source. Both beams have an angle of incidence variable between 25° and 90°. In addition to particle bombardment, 21.22-eV photons can be directed onto the target from a Vacuum Generator He lamp for UV photoelectron spectroscopy. The target can be rotated 180° to face either a triple quadrupole mass spectrometer (TQ) or a cylindrical mirror electron energy analyzer (CMA).

The preparation chamber is pumped by a 220 L/s Leybold Hereaus turbomolecular pump and has a base pressure of 4×10^{-8} Torr. The main chamber and the triple quadrupole chamber are each pumped by a Varian VK-12 cryopump and have base pressures of 4.5×10^{-10} Torr, as measured by Bayard-Alpert gauges. The FAB and ion guns are differentially pumped by a single Balzer 100 L/s turbomolecular pump with a base pressure less than 10^{-8} Torr. The entire system is bakeable to about 100 °C.

The triple quadrupole mass spectrometer[22] is home-built from commercial parts supplied by Extrel Inc. and consists of three sets of 0.95 × 20 cm rods. The first and third sets are used for mass analysis and have a mass range of 2–1000 amu. By means of capacitive coupling to either the first or the third set of rods, radio frequency voltage is applied to the second set of rods, which are surrounded by a collision chamber with 8-mm entrance and exit apertures that also double as electrostatic lenses. Gas can be leaked into the collision chamber for collision-induced dissociation (CID) experiments. The collision chamber has a separate Bayard–Alpert gauge. A 50:1 ratio between the collision chamber pressure and the triple quadrupole chamber pressure can be maintained. An off-axis Channeltron particle multiplier is used in a pulse-counting mode for ion detection. Directly on the triple quadrupole axis and next to the multiplier is a quartz prism used to send a laser beam coaxially through the triple quadrupole for photodissociation experiments.[23,24]

Secondary ions have broad kinetic energy distributions (~1–20 eV), which can significantly reduce the mass resolution of a quadrupole filter.[25] To minimize this problem, the ions are first directed through a retarding-stop energy filter[26] ("Bessel box"). The voltage above ground applied to the retarding stop roughly corresponds to the center of the

(14) Honda, F.; Lancaster, G. M.; Fukuda, Y.; Rabalais, J. W. *J. Chem. Phys.* **1978**, *69*, 4931. Campana, J. E.; Barlak, T. M.; Colton, R. J.; DeCorpo, J. J.; Wyatt, J. R.; Dunlap, B. I. *Phys. Rev. Lett.* **1981**, *47*, 1046. Barlak, T. M.; Wyatt, J. R.; Colton, R. J.; DeCorpo, J. J.; Campana, J. E. *J. Am. Chem. Soc.* **1982**, *104*, 1212. Baldwin, M. A.; Proctor, C. J.; Amster, I. J.; McLafferty, F. W. *Int. J. Mass Spectrom. Ion Processes* **1983**, *54*, 97.

(15) Jonkman, H. T.; Michl, J. *J. Am. Chem. Soc.* **1981**, *103*, 733. Orth, R. G.; Jonkman, H. T.; Powell, D. H.; Michl, J. *J. Am. Chem. Soc.* **1981**, *103*, 6026.

(16) Fayet, P.; Wöste, L. *Surf. Sci.* **1985**, *156*, 134. Ruatta, S. A.; Hanley, L.; Anderson, S. L. *Chem. Phys. Lett.* **1985**, *122*, 410. Hanley, L.; Anderson, S. L. *Chem. Phys. Lett.* **1987**, *137*, 5. Hanley, L.; Ruatta, S. A.; Anderson, S. L. *J. Chem. Phys.* **1987**, *87*, 260.

(17) Estel, J.; Hoinkes, H.; Kaarmann, H.; Nahr, H.; Wilsch, H. *Surf. Sci.* **1976**, *54*, 393.

(18) Magnera, T. F.; David, D. E.; Michl, J. *J. Am. Chem. Soc.* **1987**, *109*, 936.

(19) Kebarle, P. *Annu. Rev. Phys. Chem.* **1977**, *28*, 445. Lau, Y. K.; Ikuta, S.; Kebarle, P. *J. Am. Chem. Soc.* **1982**, *104*, 1462.

(20) Andersen, C. A.; Hinthorne, J. R. *Science* **1972**, *175*, 853.

(21) Magnera, T. F.; David, D. E.; Tian, R.; Stulik, D.; Michl, J. *J. Am. Chem. Soc.* **1984**, *106*, 5040.

(22) Yost, R. A.; Enke, C. G. *J. Am. Chem. Soc.* **1978**, *100*, 2274. Yost, R. A.; Enke, C. G. *Anal. Chem.* **1979**, *51*, 1251A.

(23) (a) Vestal, M. L.; Futrell, J. H. *Chem. Phys. Lett.* **1974**, *28*, 559. (b) McGilvery, D. C.; Morrison, J. D. *Int. J. Mass Spectrom. Ion Phys.* **1978**, *28*, 81.

(24) David, D. E.; Magnera, T. F.; Tian, R.; Stulik, D.; Michl, J. *Nucl. Instrum. Methods Phys. Res.* **1986**, *B14*, 378.

(25) Wittmaack, K. *Vacuum* **1982**, *32*, 65.

(26) Allen, J. D., Jr.; Durham, J. D.; Schweitzer, G. K.; Deeds, W. E. *J. Electron Spectrosc. Relat. Phenom.* **1976**, *8*, 395.

filter band-pass. The width of the band-pass is adjustable but is normally about 1 eV (fwhm). All lenses and the dc offsets of the three quadrupoles are referenced to the voltage applied to the retarding stop.

Data collection, storage, and handling are done by a DEC LSI 11/73 computer interfaced to the triple quadrupole via an Extrel Interlink Model 377-2.

Materials. All metal salts were reagent grade, and aqueous solutions were made with ultrahigh-purity triply distilled water. Solution storage and transfer were done in plastic containers. Rare gases for the ion and FAB guns and collision target were Matheson Research Grade. Research-grade butane (Philips) was also used as a collision target gas. Pure metals were obtained from AEsar and were Puratronic grade whenever available.

Substrate Preparation. Frozen aqueous solutions of metal salts were prepared in the concentration range of 10^{-7}–1 M. These solutions were quickly frozen onto a clean copper cryostat or Helitran tip, which was precooled to −50 °C. The solutions appeared to freeze on contact with the tip and were then further cooled to 100 K (under 1 atm of dry N_2) in the preparation chamber. The chamber was evacuated, and the sample was cooled to 20 K and positioned in the main chamber. The procedure was followed to minimize enrichment of the surface salt concentration by vacuum pumping. The poor electrical conductivity of the substrate required the use of a low-energy (<5 V) electron flood gun for optimal signal intensity of the secondary ions.

Hydrated metal salts were used by forming them into 2-mm-thick pellets with a standard laboratory press. They were fastened to the cryostat tip with Torr Seal applied between the pellet and the tip, masked by aluminum foil, and cooled to 70 K to prevent dehydration while under vacuum.

Frosted metal surfaces were prepared at first by direct deposition of 10^4–10^5 monolayers of water vapor onto the cold surface of a thin sheet of a pure transition metal. The sample was then sputtered until metal ion and hydrated metal ion signals were obtained. Concurrent with this change is a decrease in value of the maximum of the secondary ion kinetic distribution from above 10 eV to 2 eV. Eventually the flood gun can be turned off with no effect on the signal or location of the kinetic energy maximum. As the substrate becomes thinner, the signals of $M^+(H_2O)_n$ steadily increase, reach a maximum, and decline to a nearly steady intensity, which then only decreases very slowly with time. Hydrated metal ions are detectable within 10 min, and a usable signal is obtained for several hours.

In place of a single deposition of water vapor, a dynamic system was subsequently devised that enhanced the hydrated metal ion signal. A low-density jet of water vapor was directed onto the surface of a cooled metal (180 K). When the flow of water vapor was adjusted, the intensity of a particular $M^+(H_2O)_n$ cluster signal could be maximized and maintained at a steady level. Also by this method, it was possible to produce clusters of the type Cu^+L_n and $Cu^+(H_2O)L$ by introducing a 10:1 mixture of Ar or N_2 and H_2O and lowering the temperature to 20 K. Only weak signals for $Cu^+(H_2O)_nL_m$ clusters were observed for either n or $m > 1$.

When the target is at room temperature, the secondary ion yield of $Cu^+(H_2O)$ and $Cu^+(H_2O)_2$ was enhanced by the presence of H_2O vapor. The enhanced signal increased with H_2O pressure until it saturated at a main chamber pressure above 5×10^{-5} Torr.

Hydration Energy Measurements. In a collision-induced dissociation experiment, the first quadrupole mass filter is used to select a single parent cluster ion, which is introduced into the collision chamber with a variable axial kinetic energy. Collision chamber pressures are chosen such that the parent ion undergoes at most one inelastic collision during which it can accept as internal energy some fraction of the total energy of the collision system. The energy transferred may be localized to a specific bond or may be accessible throughout the parent cluster ion. If this energy is sufficient, one or more cluster constituents will be ejected, leading to the formation of daughter ions of smaller mass. If this occurs within approximately 100 μs, the daughter ions will be efficiently collected by the radio frequency quadrupole fields and injected into the third set of quadrupole rods, which serve to mass analyze the daughter ions. Figure 2 shows the results of such an experiment where $Cu^+(H_2O)_4$ undergoes collisions with n-butane at laboratory energies between 0 and 15 eV. The collision energy in the laboratory frame is taken as the difference between the potential applied to the retarding stop of the Bessel box and that applied to the quadrupole rods plus the entrance and exit lenses that define the collision chamber. The total collision energy of the system, in addition to that obtained by dc acceleration, includes the inherent kinetic energy distributions both of the parent ion passed by the Bessel box and of the target gas[27] (Doppler broadening), their internal energy distributions, and any contributions by the collision chamber quadrupole radio frequency field. The kinetic energy distribution of the

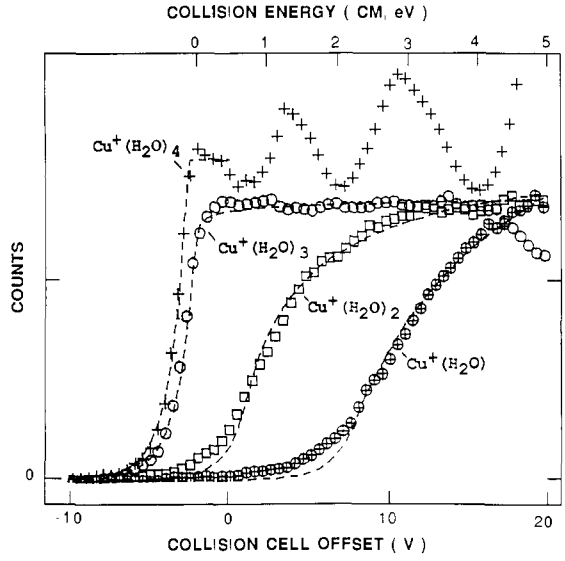

Figure 2. Excitation curves for collision-induced dissociation of $Cu^+(H_2O)_4$ in Ar. The pressure in the collision chamber was 5×10^{-5} Torr. The dashed lines are fitted excitation curves.

parent ion is a function of the 1-eV fwhm Bessel box band-pass. Doppler broadening, resulting from target gas motion, and its effect on low-energy collisions have been previously discussed.[27] At 300 K it is typically around 0.2 eV for a nominal center of mass collision energy of 2 eV. The radio frequency fields in the collision chamber contribute an unknown amount to the collision energy. At 1.2 MHz, the radio frequency contribution for a quadrupole field is expected to be small. Even for the worst case, ions entering far off axis, it will be less than 1 eV for an ion of 100 amu, based on multipole theory[6a,28,29] and trajectory calculations.[23b]

The ion intensities in Figure 2 are not normalized to total ion signal but rather are presented as raw counts. This is done to avoid introducing the focusing effects of radio-frequency-only quadrupoles on transmitted ions.[30] The focusing effects are evident in the parent ion signal as intensity oscillation as a function of ion velocity, i.e., collision energy in Figure 2. They are manifested strongly only by those ions that travel without collisions through the length of the chamber. Focusing effects are generally not strongly apparent in the daughter ion signals because they have neither a common origin along the axis of the collision chamber nor a narrow axial energy distribution.

The collision chamber quadrupole rods function as a highly efficient retarding field energy analyzer if their offset potential is raised above that of the Bessel box energy analyzer. The action of the collision chamber rods as an energy analyzer is evident in the steeply rising parent ion intensity as the dc offset is increased in the vicinity of 0 V. The intensity plot represents the integrated form of the kinetic energy distribution of ions transmitted by the Bessel box analyzer. The band-pass distribution of the Bessel box was found to be well represented by the arbitrarily selected functional form $x^s \exp(-\beta x)$. A least-squares fit of the function $I_{max}(x - V_0)^s \exp[-\beta(x - V_0)]$ to the initial parent ion intensity curve locates the zero, V_0, of the distribution and determines its width, β, where V_0 is the dc offset potential relative to the Bessel box retarding stop and I_{max} is the maximum transmitted intensity. It also determines the optimum value of the exponent, s.

A characteristic of Figure 2 is the coincident appearance of the parent ion $Cu^+(H_2O)_4$ and the first daughter ion, $Cu^+(H_2O)_3$, as the collision energy is increased. This is typical of all the collision energy profiles generated by sputtered parent ions that we have examined thus far. A similar set of curves have been previously reported for protonated water clusters[31] generated in a high-pressure ion source. These curves show a nearly vanishing apparent energy difference between the parent ion and first daughter ion. Calculations[32] of the thermal internal energy distri-

(27) Chantry, P. J. *J. Chem. Phys.* **1971**, *55*, 2746.

(28) Teloy, E.; Gerlich, D. *Chem. Phys.* **1974**, *4*, 417.

(29) Landau, L. O.; Lifshitz, E. M. In *Mechanics*, 3rd ed.; Pergamon Press: New York, 1976; p 93. Dehmelt, H. G. In *Advances in Atomic and Molecular Physics*; Bates, D. R., Estermann, I., Eds.; Academic Press: New York, 1967; Vol. 3, p 53.

(30) *Quadrupole Mass Spectrometry and its Applications*; Dawson, P. H., Ed.; Elsevier: New York, 1976.

(31) DePaz, M.; Leventhal, J. J.; Friedman, L. *J. Chem. Phys.* **1968**, *49*, 5543. DePaz, M.; Leventhal, J. J.; Friedman, L. *J. Chem. Phys.* **1969**, *51*, 3748.

butions and lifetimes of small ground-state clusters indicate that, for about three or more ligands, energy slightly in excess of an ion–ligand bond is easily stored for several hundred microseconds before unimolecular decomposition occurs.

Cluster ions formed by sputtering have been observed to be metastable.[33] In our experience a small fraction of nearly all cluster ions generated by sputtering exhibits unimolecular decomposition within the 100-μs time frame of our experiments. This fraction is strongly dependent on cluster size and can range from less than 1% to nearly 10%. Usually, it rises slightly as the Bessel box band-pass is adjusted to select cluster ions initially ejected with a higher velocity. We believe that this general metastability arises from energy stored randomly within the modes of intermolecular motion and the lower frequency intramolecular vibrational modes of the cluster's molecular constituents. The cluster can be described as "warm" and represents the final stage of the process which generates these cluster ions by ejection of material from the original impact region, initially at a very high "temperature", and rapidly cooled by evaporative loss of the least firmly held constituents.[24,34] Ions that are metastable must have internal energy distributions that extend above the dissociation limit of the weakest bond in the cluster. Given this, the first daughter ion should appear simultaneously with the parent ion and its threshold should be coincident with the collision energy zero of the system as observed. The close similarity of the low-energy parts of the parent and daughter ion excitation curves is an indication of the large number of populated states just below the dissociation limit. It is quite possible that all internal states are equally likely, i.e., that the internal energy distribution follows the state density function; it certainly is not a Boltzmann distribution.

Product ions generated in collision-induced dissociation experiments in a triple quadrupole are collected very efficiently, making detection of reactions with small cross-sections possible. The effective cross-section for a reaction is defined by

$$\sigma_{eff}(E) = \int F(\epsilon,E)\ \sigma(\epsilon)\ d\epsilon \qquad (1)$$

where E is the nominal center of mass collision energy, $F(\epsilon,E)$ is the actual distribution of energies about E, and the integration is done over the appropriate range of ϵ, which is related to x by $\epsilon = V_0 - x$. The energy-dependent cross section $\sigma(\epsilon)$ usually assumed in the interpretation of experiments of this kind is $\sigma_0(\epsilon - E_0)^n/\epsilon^m$ for an endoergic process.[5f,6b,35] The values of n and m have been found to have a wide range of values, both empirically and theoretically. Models that have been used include direct collisions,[35a,b] statistical,[35c] and phase space.[35d] A more detailed account can be found in ref 6b. For dissociation reactions, the empirically determined range of n is 1.5–2.3 when m is set equal to unity[6c,35e] and 1.0–2.0 when m is set equal to 0.5. In cases where the parent ion kinetic energy distribution is monoenergetic, $F(E,\epsilon)$ is the distribution of relative translational energy of the target gas.[27] More elaborate treatments include the kinetic energy distribution of the parent ions.[36] In our experiment, the parent ion kinetic energy distribution is fairly broad and represents the most significant contribution to $F(E,\epsilon)$. When target gas motion is neglected and when eq 1 and the empirical forms of the kinetic energy distribution and of the endoergic cross section are used, the effective cross section becomes

$$\sigma_{eff}(E) = \sigma_0 \int_0^{E_{max}} (\epsilon + E - E_0)^n (\epsilon + E)^{-m} (\epsilon)^s\ u(\epsilon) e^{-\beta(\epsilon)}\ d\epsilon \qquad (2)$$

with $u(\epsilon)$ defined by

$$u(\epsilon) = 0 \quad \text{if } \epsilon < E_0 - E$$

$$u(\epsilon) = 1 \quad \text{if } \epsilon > E_0 - E$$

where E_0 is the threshold and s and β are constants characterizing the width of the reactant kinetic energy distribution and determined from the fit of the parent ion intensity plot as explained earlier. Equation 2 can be fitted by a nonlinear least-squares procedure to the observed daughter ion excitation function giving values of σ_0, m, n, and E_0. It was generally found that eq 2 did not fit the data very well and resulted in values of E_0 that were too large, in particular, for the smallest daughter ion. It was found, however, that eq 2 could be modified to fit all the data well and reproduce known values of E_0, if $n = m = 1.5$ and the data points used in the fit were restricted to those in the rising position of the excitation function. Inclusion of the data points in the decreasing portion of the excitation function required that $m > n$ in eq 2 and was the source for the values E_0 that were too large. The value of n was kept constant during the fit. The ad hoc choice of $n = m = 1.5$ is the result of an extensive search for a form of the cross section $\sigma(\epsilon)$ that would reproduce all data for which comparison with reported values was possible. The search included concave, linear, and convex forms for $\sigma(\epsilon)$, at times convoluted explicitly with various assumed forms of the internal energy distribution of the cluster.

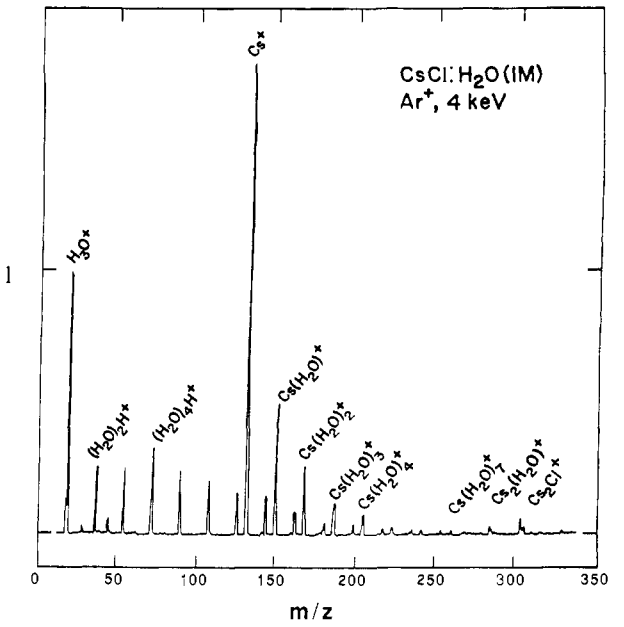

Figure 3. SIMS spectrum of a frozen aqueous solution of 1 M CsCl.

Results

Secondary Ion Mass Spectra. There are no significant differences between the mass spectra obtained using incident ions or fast atoms. Bare metal ions were detected in the spectra of all the frozen aqueous salt solutions examined. Signals were the strongest for salts of the alkali and alkaline earth metals. For these, bare metal ion signals were obtained readily on 10^{-7} M solutions. The signals were the weakest for salts of second- and third-row metals such as Cd, Hg, and Pb; 10^{-1} M solutions were required for good quality spectra. As observed for frozen gas targets,[15] cluster formation was promoted by the use of relatively heavy incident ions or atoms such as Ar^+ or Ar and was negligible for light incident ions such as He^+. Intensity patterns for extensively hydrated alkali-metal ions varied from exponentially decreasing for Cs^+ to gently rising and then decreasing for Li^+.

In discussing the cluster ions in the following, we frequently refer to the oxidation state of the metal as if it were known with certainty once the total cluster composition is known. In reality, such simple correspondence exists only if the water ligands are preserved intact, i.e., if the metal ion does not insert into an OH bond. Often, this is a reasonable assumption, but we use the same notation throughout for simplicity and refer to an $M^+(H_2O)$ ion as a cluster of the univalent metal M(I) as if we knew that the structure is $M^+\cdots OH_2$ as opposed to $H-M^+-OH$, which corresponds to the trivalent M(III). Particularly for the early transition metals, our formal designation need not correspond to the real cluster structure.

Examples of positive secondary ion spectra are presented in Figures 3–6 for each substrate type. In Figures 3 and 4, secondary ion spectra of frozen aqueous solutions of 1 M CsCl and 0.1 M

(32) Sunner, J.; Kebarle, P. *J. Phys. Chem.* **1981**, *85*, 327.
(33) Magnera, T. F.; David, D. E.; Michl, J. *Chem. Phys. Lett.* **1986**, *123*, 327.
(34) Michl, J. *Int. J. Mass Spectrom. Ion Phys.* **1983**, *53*, 255. Urbassek, H. M.; Michl, J. *Nucl. Instrum. Methods Phys. Res.* **1987**, *B22*, 480.
(35) (a) Maier, W. B., II *J. Chem. Phys.* **1964**, *41*, 2174. Maier, W. B., II *J. Chem. Phys.* **1965**, *42*, 1790. (b) Levine, R. D.; Bernstein, R. B. *Chem. Phys. Lett.* **1971**, *11*, 552. Menziger, M.; Yokozeki, A. *Chem. Phys.* **1977**, *22*, 273. Levine, R. D.; Bernstein, R. B. *J. Chem. Phys.* **1972**, *56*, 2281. (c) Rebick, C.; Levine, R. D. *J. Chem. Phys.* **1973**, *58*, 3942. Morokuma, K.; Eu, B. C.; Karplus, M. *J. Chem. Phys.* **1969**, *51*, 5193. (d) Moran, T. F.; Fullerton, D. C. *J. Chem. Phys.* **1971**, *54*, 5231. Chesnavich, W. J.; Bowers, M. T. *J. Phys. Chem.* **1979**, *83*, 900. (e) Parks, E. K.; Wagner, A.; Wexler, S. *J. Chem. Phys.* **1973**, *58*, 5502.
(36) Lifshitz, C.; Wu, R. L. C.; Tiernan, T. O.; Terwilliger, D. T. *J. Chem. Phys.* **1978**, *68*, 247.

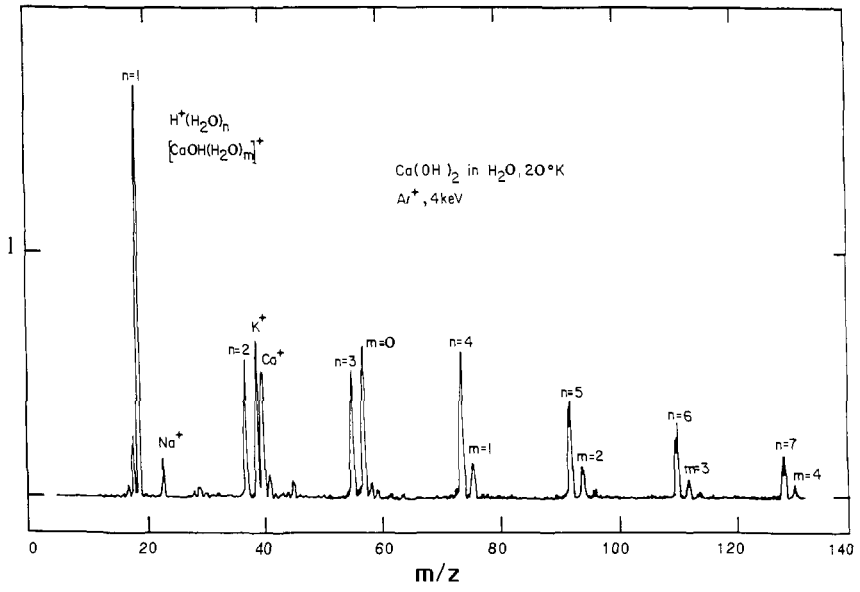

Figure 4. SIMS spectrum of a frozen aqueous solution of 0.1 M $Ca(OH)_2$.

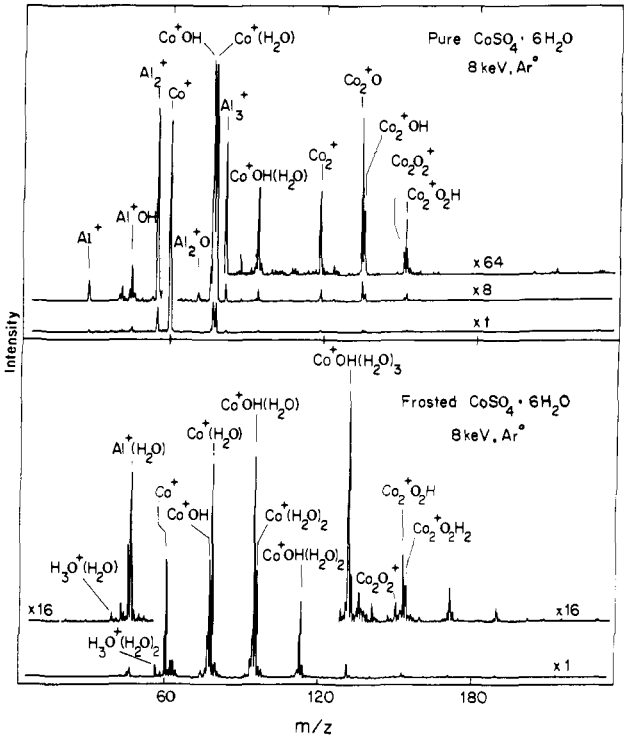

Figure 5. SIMS spectrum of a pressed pellet of pure $CoSO_4 \cdot 6H_2O$ (top). SIMS spectrum of the same target except frosted with H_2O (bottom).

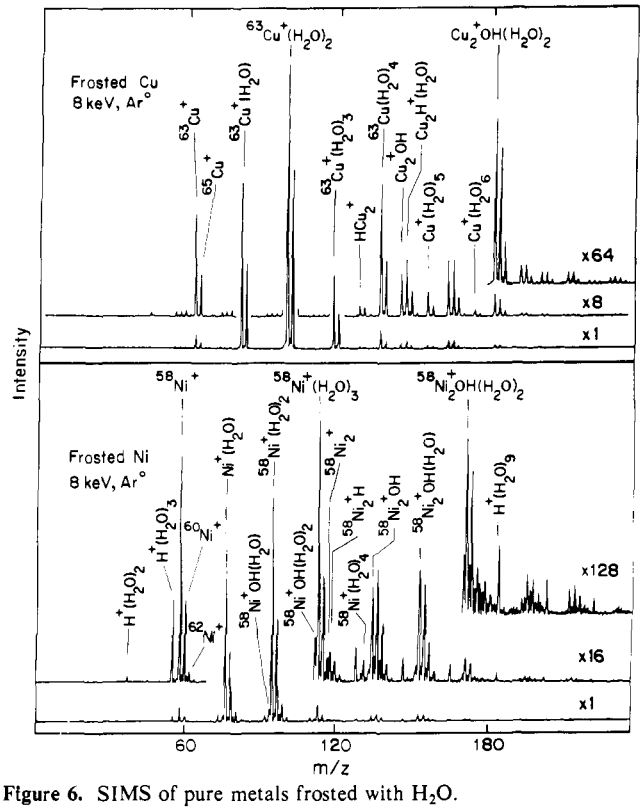

Figure 6. SIMS of pure metals frosted with H_2O.

$Ca(OH)_2$ are compared. The SIMS of CsCl has $Cs^+(H_2O)_n$ as the predominant series along with weaker $Cs_2^+(H_2O)_n$ and $H^+(H_2O)_n$ series. At lower concentrations or with lighter primary ions such as He^+, the $Cs_2^+(H_2O)_n$ series is absent. In contrast, the cluster series $Ca^+(H_2O)_n$ is never observed in the SIMS of frozen aqueous $Ca(OH)_2$, and the series $Ca^+OH(H_2O)_n$ and $H^+(H_2O)_n$ are present instead. No series of the types $Ca_2^+X_mY_n$ or $Ca_2^+X_n$ are observed. However, the SIMS of frozen solutions of salts of first-row transition metals of groups IV–VIII can simultaneously have signals for the $M^+(H_2O)_n$ and the $M^+OH(H_2O)_n$ series. An electron flood gun was always required with these substrates to obtain a strong signal.

The SIMS results for pure and slightly frosted $CoSO_4 \cdot 6H_2O$ are presented in Figure 5. The unfrosted target has strong signals for the Co(I) ion $Co^+(H_2O)$ and the Co(II) ion Co^+OH, and weaker signals for $Co^+OH(H_2O)$, Co_2^+, Co_2^+O, etc., but the dominant signal is the bare metal ion. Relatively much stronger signals for the Co(I) series $Co^+(H_2O)_n$ and the Co(II) series $Co^+OH(H_2O)_n$ are observed for the frosted target. Both series show sharp decreases in signal intensity after two ligands have been attached to the metal ion. The SIMS of the frosted target also shows an increased Co(I)/Co(II) ratio relative to the unfrosted salt target; for instance, $Co^+(H_2O)/Co^+OH$ goes from 1:1 to 2:1. In a similar fashion, $Co_2^+O_2H/Co_2^+O_2$ changes from 2:1 to 4:1. The bare metal ions and dimer signals have at the same time been substantially reduced by conversion in the presence of more H_2O to $Co^+(H_2O)$, $Co^+OH(H_2O)$, $Co_2^+O_2H$, etc. The ions containing aluminum are generated by the peripheral portions of the unfocused FAB beam striking the aluminum mask.

Figure 6 shows contrasting SIMS spectra obtained from frosted Cu and Ni surfaces. Both have the $M^+(H_2O)_n$ series to at least $n = 4$ or beyond, and both show an intensity break after two ligands have been attached. Copper does not, however, yield the Cu(II) series $Cu^+OH(H_2O)_n$, in contrast with Ni and other

Table I.[a] Successive Proton Hydration Energies for $H^+(H_2O)_{n-1} + H_2O \rightarrow H^+(H_2O)_n$

parent ion	$\Delta E_{1,2}$	$\Delta E_{2,3}$	$\Delta E_{3,4}$	$\Delta E_{4,5}$
$H^+(H_2O)_3$	30 ± 3			
$H^+(H_2O)_4$	32 ± 4	20 ± 3		
$H^+(H_2O)_5$		23 ± 4	18 ± 3	
$H^+(H_2O)_6$			16 ± 4	12 ± 4
lit.[b]	31.0	18.6	17.3	12.1

[a] All values in kcal/mol. [b] Reference 19; these values have been converted from ΔH^{298} to ΔE^{298}.

transition metals that we have investigated.

The solvation of the metal ion dimers of Cu and Ni is more complicated and includes series of the types $M_2^+H(H_2O)_n$, $M_2^+OH(H_2O)_n$, and $M_2^+O(H_2O)_n$, with negligible intensity for $M_2^+(H_2O)_n$.

Succesive Hydration Energies of $H^+(H_2O)_n$. Before using our procedure for the determination of unknown hydration energies, we have tested it on two cases for which good literature data are already available. One of these is characterized by small and one by large binding energies.

Successive hydration energies $\Delta E_{n-1,n}$ of $H^+(H_2O)_n$ are defined by

$$H^+(H_2O)_{n-1} + H_2O \rightarrow H^+(H_2O)_n \qquad (3)$$

and can be obtained from the reverse collision-induced dissociation steps

$$\begin{aligned}
&H^+(H_2O)_n + A \rightarrow H^+(H_2O)_{n-1} + H_2O + A && -\Delta E_{n-1,n}\\
&H^+(H_2O)_n + A \rightarrow H^+(H_2O)_{n-2} + 2H_2O + A && -\Delta E_{n-2,n}\\
&\quad\vdots \qquad\qquad \vdots \qquad\quad \vdots && \quad\vdots\\
&H^+(H_2O)_n + A \rightarrow H^+(H_2O)_{n-m} + mH_2O + A && -\Delta E_{n-m,n}\\
&\quad\vdots \qquad\qquad \vdots \qquad\quad \vdots && \quad\vdots\\
&H^+(H_2O)_n + A \rightarrow H^+ \qquad + nH_2O + A && -\Delta E_{m,n} \qquad (4)
\end{aligned}$$

where A is the collision gas, or from the difference

$$\Delta E_{n-1,n} = \Delta E_{n-m-1,n} - \Delta E_{n-m,n} \qquad (5)$$

Table I lists the $\Delta E_{n-1,n}$ values we have obtained for $H^+(H_2O)_n$ (n = 2–5) and shows that they agree with the values $\Delta E^{298}_{n-1,n}$ obtained from the reported[19] high-pressure mass spectrometry values of $\Delta H^{298}_{n-1,n}$ by adding RT. Since we do not know the internal energy distributions of either the reactants or the products in eq 4, we cannot specify the nominal temperature T for which the $\Delta E_{n-1,n}$ values were determined.

Binding Energies of Co^+OH and Cr^+OH. The test of our method by comparison with the known proton hydration energies demonstrates the validity of the method for determining binding energies in the range 10–25 kcal/mol. In order to extend the test to strong bonds we examined the system

$$M^+OH(H_2O) + A \rightarrow M^+OH + H_2O + A$$

$$M^+OH(H_2O) + A \rightarrow M^+ + OH + H_2O + A \qquad (6)$$

for M = Co and Cr. The threshold difference we observe between the appearance and Co^+OH and Co^+ is 72 ± 2 kcal/mol. This is interpreted as $D(Co^+–OH)$. The hydroxide bond energy was determined from previous photodissociation experiments[8] to be 71 ± 3 kcal/mol. Following the same procedure, we obtain 74 ± 3 kcal/mol for $D(Cr^+–OH)$, which compares to the literature value of 73 ± 5[5a] kcal/mol.

Successive Hydration Energies of $Cu^+(H_2O)_n$. Having found satisfactory agreement with previously reported binding energies in both cases examined, we used our procedure to determine previously unknown binding energies. Successive hydration energies $\Delta E_{n-1,n}$ of $Cu^+(H_2O)_n$ are defined by

$$Cu^+(H_2O)_{n-1} + H_2O \rightarrow Cu^+(H_2O)_n \qquad (7)$$

and can be obtained from the reverse collision-induced dissociation steps analogous to eq 4 and 5. The $\Delta E_{n-1,n}$ values obtained this way for $Cu^+(H_2O)_n$ are listed in Table II for n = 1–4. For each parent ion it was possible to analyze several successive losses and to obtain more than one $\Delta E_{n-1,n}$. Good agreement was found for the same $\Delta E_{n-1,n}$ obtained from different parent ions, demonstrating good internal consistency between experiments. Also listed in Table II are the hydration energies $\Delta E^{298}_{n-1,n}$ previously measured[4b] for the larger clusters, n = 3,4. To obtain these from the hydration enthalpies $\Delta H^{298}_{n-1,n}$ derived from high-pressure mass spectrometry experiments, we have added RT. Our results for n = 3 and n = 4 agree within ~1 kcal/mol with the literature data.

Table II.[a] Successive Hydration Energies of Cu^+. $Cu^+(H_2O)_{n-1} + H_2O \rightarrow Cu^+(H_2O)_n$

parent ion	$\Delta E_{0,1}$	$\Delta E_{1,2}$	$\Delta E_{2,3}$	$\Delta E_{3,4}$
$Cu^+(H_2O)_2$	35 ± 3			
$Cu^+(H_2O)_3$	38 ± 5	39 ± 3		
$Cu^+(H_2O)_4$		37 ± 4	17 ± 2	
$Cu^+(H_2O)_5$			19 ± 3	15 ± 2
$Cu^+(H_2O)Ar$	35 ± 5			
$Cu^+(H_2O)N_2$	36 ± 5			
lit.[b]			15.8 ± 0.2	16.1 ± 0.2

[a] All values in kcal/mol. [b] Reference 4b; these values have been converted from ΔH^{298} to ΔE^{298}.

Another test of our method of determining the $\Delta E_{n-1,n}$ values was possible in that the value of $\Delta E_{0,1}$ was also determined from collision-induced dissociation of $Cu^+(H_2O)L$, L = Ar or N_2, and good agreement was obtained (Table II). Replacing a H_2O ligand with Ar or N_2 is expected to reduce the total random internal energy of the selected parent ions since the total amount of this energy cannot greatly exceed the dissociation limit of the weakest bond in the cluster for the 100-μs time period involved in our experiment and since Ar or N_2 are expected to be weaker ligands than water. Good agreement between the $\Delta E_{0,1}$'s indicates that the threshold method is not sensitive to the total random energy of the parent.

As we only rely on differences between excitation curves, the knowledge of the precise locations of the absolute energy zero in plots such as Figure 2 is unimportant, but we need to know the form of the energy distribution used in the deconvolution reliably. Our procedure was tested by purposely broadening the band-pass width of the Bessel box up to as much as 7 eV. Except for a greater standard deviation, there was no detectable difference in the results. Also the use of various collision gas partners (Ar, Xe, *n*-butane) had no effect on the results.

Hidden Sources of Error. The precision of this method is estimated to be ±3 kcal/mol (1 standard deviation). Systematic errors might arise from the following: (i) an energy barrier to the dissociation process; (ii) internal energy carry-over; (iii) lateral motion induced by the radio frequency field; (iv) detection of ionic products only; and (v) differences in electronic excitation. We shall consider these one at a time.

(i) Ion–molecule association reactions are generally believed to proceed without activation energy. The minimum energy required to observe the reverse dissociation process should be the true dissociation limit plus a small excess to ensure that the energized ion will fragment within the about 100-μs residence time in the quadrupole. Since all observed daughter ions will require approximately this same small amount of energy in excess of D_0, the difference procedure used here should largely cancel this source of error.

(ii) In the absence of a reaction barrier above D_0 in the reaction path it is expected that internal energy carry-over and/or anomalous kinetic energy release will not be a serious problem. This is confirmed by the good agreement between binding energies determined from different parent ions.

(iii) Lateral motion induced by the radio frequency field shifts slightly the kinetic energy of the collisions. The difference method used here makes this energy component indistinguishable from the internal energy contained in the parent ion.

(iv) It is assumed in the analysis that losses of several water molecules from a cluster ion that has been highly energized by

Table III.[a] Estimated Reaction Enthalpies[b]

reaction	M					
	Ca	Cr	Fe	Co	Ni	Cu
$M^{2+} + H_2O \rightarrow M^+ + H_2O^+$	17	−85	−83	−103	−128	−177
$M^{2+} + H_2O \rightarrow M^+OH + H^+$	52	−17	−13	−32	−29	>−78[c]
$M^+ + H_2O \rightarrow M^+OH + H^\bullet$	16	46	46	48	76	>76[c]
$M^0 + H_2O^+ \rightarrow M^+ + H_2O$	−150	−135	−111	−111	−115	−113
$M^0 + H_2O^+ \rightarrow M^+OH + H^\bullet$	−134	−90	−64	−62	−39	>−37[c]
$M^+ + H_3O^+ \rightarrow M^+OH + H_2$	−91	−47	−21	−20	−4.1	>6.2[c]
$M^+OH \rightarrow M^+ + OH$	−106[d]	73[b,f]	73[b,e]	71[a,e,f]	42[g]	

[a] All values in kcal/mol. [b] As determined from data found in: *Ionization Potentials, Appearance Potential, and Heats of Formation of Gaseous Positive Ions*; U.S. Department of Commerce. National Bureau of Standards, NSRDS-NBS 26; U.S. Government Printing Office: Washington, DC 1982. [c] Estimated assuming $D(Cu^+–OH) < D(Ni^+–OH)$. [d] Murad, E. *J. Chem. Phys.* **1981**, *75*, 4080. [e] Reference 8. [f] This work. [g] Magnera, T. David, D. E.; Michl, J. *J. Am. Chem. Soc.* **1989**, *111*, 4100.

a collision are fast but sequential. Since the neutral fragments are not detected, one needs to consider the possibility that they consist of clusters of two or more water molecules. For such a case, our thresholds would be lower by an amount corresponding to the binding energy of the neutral cluster. This would lead to a systematic discrepancy between overlapping bond dissociation energies measured starting with different parent cluster ions. This was not observed (Tables I and II).

(v) It is possible that the metal in the parent cluster ion is electronically exicted at the time of collision. Considering the time scales involved, this is a potential complication only if conversion to the ground electronic state is multiplicity forbidden. It is also possible that the parent cluster ion is initially in its electronic ground state but that the collision produces an electronically excited daughter ion. This is only likely if the multiplicities of the ground states of the parent and daughter ions differ and the parent multiplicity fails to change during the short time of the collision and fragmentation period.

As shown in Figure 7, the physical significance of the measured binding energy will vary depending on the answers to three questions. First, is the parent ion excited? Second, does multiplicity change as a result of the collision? Third, is the multiplicity of the two ground states the same? If the answers are not known, it need not be obvious what has actually been measured. The probability of possible confusion is reduced if the same results are obtained starting with several different parent ions. Since this has been observed in our case and since our excitation curves contain no multiple steps or other irregularities attributable to the occupancy of two or more energetically separated electronic states in the parent ions, we believe that the case of $Cu^+(H_2O)_n$ is free of such ambiguities. This is not very surprising considering that the Cu^+ ion has a relatively high excitation energy.[37] However, caution is clearly required in the case of ions with low-lying states of multiplicity different from that of the ground state, such as Fe^+.[37]

In summary, barring complications with close-lying states of different multiplicity, we believe that the accuracy of binding energy determination by our procedure is comparable to its precision, about ±3 kcal/mol, as judged by comparison of data obtained from different starting cluster ions and by comparison with independent values reported in the literature.[5a,8,19]

Discussion

Nature of the Secondary Ions. The SIMS spectra of the three types of substrates extend the original work on frosted LiF[17] crystals considerably. The spectra in the present work show a richer variety of ions. In particular, metals that commonly occur in higher oxidation states form (assumed) divalent metal series $M^+OH(H_2O)_n$ in addition to the (assumed) monovalent metal series $M^+(H_2O)_n$. The intensity ratio M(II)/M(I) decreases in the order Ca > Cr > Fe > Co > Ni > Cu, Cs. This ratio is independent of the original oxidation state of the metal in the target substrate, in keeping with the hydrodynamic flow ejection mechanism proposed for the formation of these clusters.[24,35] Rapid

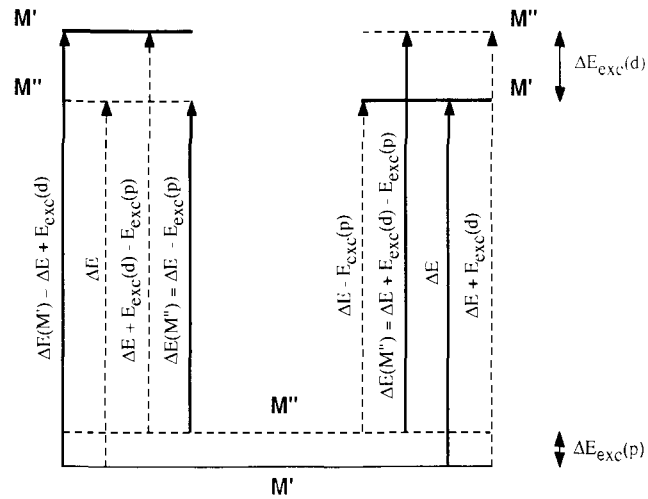

Figure 7. Collision-induced dissociation of parent ions (eq 7) in initial electronic states of multiplicities M′ and M″, separated by excitation energy $E_{exc}(p)$, forming daughter ions in final electric states of multiplicities M′ and M″, separated by excitation energy $E_{exc}(d)$, either arranged in the same (right-hand side) or the opposite (left-hand side) order as those of the parent ion. The quantities that may result from binding energy determination are indicated by vertical arrows: full line, multiplicity conserved; broken line, multiplicity changed in the CID process. ΔE: equilibrium solvation energy. $\Delta E(M')$ and $\Delta E(M'')$: adiabatic solvation energies in states of multiplicity M′ and M″, respectively.

charge exchange is expected to occur in the hot supercritical gas generated in the impact region surrounding the path of the incident ion, transferring the positive charge to carriers with the lowest ionization potential.[38]

Doubly charged metal ions will be removed by reducing reactions such as

$$M^{2+} + H_2O \rightarrow M^+ + H_2O^+$$
$$M^{2+} + H_2O \rightarrow M^+OH + H^+$$
$$M^{2+} + M \rightarrow 2M^+$$
$$M^{2+} + e^- \rightarrow M^+$$
$$\text{etc.} \qquad (8)$$

Zero-valent metal atoms can be oxidized in reactions such as

$$M^0 + H_2O^+ \rightarrow M^+ + H_2O$$
$$M^0 + H_2O^+ \rightarrow M^+OH + H^\bullet$$
$$M^0 + H_3O^+ \rightarrow M^+(H_2O) + H^\bullet$$
$$M^0 + H_3O^+ \rightarrow M^+OH + H_2$$
$$M^0 + H^+ \rightarrow M^+ + H^\bullet \qquad (9)$$

and singly charged ones in the process

(37) Moore, C. E. *Atomic Energy Levels*. NSRDS-NBS 35; National Bureau of Standards: Washington, DC, 1971; Vol. II.

(38) Orth, R. G.; Jonkman, H. T.; Michl, J. *J. Am. Chem. Soc.* **1982**, *104*, 1834.

$$M^+ + H_2O \rightarrow M^+OH + H^\bullet \quad (10)$$

In addition, oxidative addition to O–H bonds can occur.

Estimates of the ΔH's for the above oxidation/reduction reactions between water and various metals are summarized in Table III. It is clear that bare doubly charged metal ions are unlikely to exist after only a few collisions with water molecules. Most will be able to oxidize water via a simple charge exchange or elimination of H^+. For example, copper(II) can do both, but oxidation of water will be strongly favored. Singly charged metal ions are thermodynamically stable in the presence of water and will not be oxidized to M^+OH. Zero-valent metals will be oxidized by H_2O^+ to form M^+OH unless the metal ion forms relatively weak M–OH bonds as is the case for Cu and Ni. Zero-valent metal clusters are even more reducing than single atoms and must form very strong bonds to hydroxyl because only $M_2^+OH(H_2O)_n$ and no $M_2^+(H_2O)_n$ clusters have been observed. Metal ions will be generated along with atoms from frosted metal targets, but the ratio $M^+OH/M^+(H_2O)$ will be controlled by the degree of oxidation of the neutrals to M^+OH. This will, in turn, be controlled by the M^+–OH bond strength. The observed ratio M^+-$OH/M^+(H_2O)$ qualitatively follows the reaction enthalpies listed in Table III for the reaction $M^0 + H_2O^+ \rightarrow M^+OH + H$. Sputtered bivalent metal salts either neat or frozen in solution are a good source of $M^+OH(H_2O)_n$, with the lone exception of Cu. It is in general difficult to choose a substrate that will exclusively lead to $M^+(H_2O)_n$ or $M^+OH(H_2O)_n$ clusters, and we have succeeded only in exceptional cases such as the alkali and rare earth metals and copper.

Hydration Energies. The utility of ion and fast atom bombardment for the production of metal ion clusters is demonstrated on the measurement of the successive hydration energies. The trend in the hydration energies of $Cu^+(H_2O)_n$ as a function of n is interesting: $\Delta E_{0,1}$ and $\Delta E_{1,2}$ are approximately the same within experimental error and the third, fourth, and fifth hydration energies are very close to each other, but they are less than half of the first two. This is comparable to but much more dramatic than the previous results for the Ag^+–H_2O system.[4c]

Copper is the only first-row transition metal that has an extensive aqueous chemistry in the 1+ oxidation state. The Cu^+ ion is unstable, however, relative to dismutation into Cu(0) and Cu(II) in the absence of complexing ligands. It forms dicoordinated linear complexes with ligands.[39] This is assumed to be due to the similarity between the energies of the 4s and 3d orbitals. The pronounced decrease in the hydration energy of the third and higher water ligands strongly suggests that gas-phase Cu^+ also prefers dicoordinated complexes. It is possible to speculate from the peak intensity patterns observed in the SIMS of frosted $CoSO_4$ and Co metal that dicoordination is preferred for the monovalent Co^+ ions as well.

(39) Cotton, F. A.; Wilkinson, G. In *Advanced Inorganic Chemistry: A Comprehensive Text*; Interscience: New York, 1976.

The second hydration energy of Cu^+ is large. It exceeds that of Sr^+, formerly the strongest known metal ion–water bond,[3b] by more than 4 kcal/mol. It is surprising that it may be greater than the first hydration energy. This bond strength is consistent with the previous failure to measure the equilibrium constant for the reaction

$$Cu^+(H_2O) + H_2O \rightleftarrows Cu^+(H_2O)_2 \quad (11)$$

at temperatures up to 400 °C.[4] The presence of any excited electronic states would reduce the observed hydration energy relative to the true value. The large value is then indirect evidence that excited states of Cu^+ do not represent a serious complication in the measurements.

Possible Analytical Utility. The sensitivity of detection of ions sputtered from a frozen H_2O matrix depends considerably on the nature of the ions; 10^{-5}–10^{-6} M solutions have been used. We are not certain, however, if this high sensitivity is intrinsic or the consequence of unintentional surface enrichment. Surface enrichment might arise from several possible causes such as microcrystal formation, concentration gradients introduced during the freezing process or differential sputtering rates. With careful preparation, however, it should be possible to measure properties of ions in solution, such as dissociation constants, pH dependence of aggregation, chelation, etc., by quantitative determination of the sputtered products. Already thermodynamic data have become available by similar techniques applied to fast atom bombardment of ions in a liquid-phase glycerol/water matrix.[40]

Conclusions

Ion and fast atom bombardment has been demonstrated to be a convenient and versatile method for the production of hydrated transition-metal ions. When combined with collision-induced dissociation methods, this cluster ion source provides access to successive hydration energies. Agreement between the hydration energies of $H_3O^+(H_2O)_n$ and $Cu^+(H_2O)_n$ and the hydroxide bond energies in Co^+OH and Cr^+OH measured here and those measured previously by well-established techniques underscores the reliability of this method. Further, new measurements of $\Delta E_{0,1}$ and $\Delta E_{1,2}$ when compared with successive ΔE's give strong evidence that Cu^+ preferentially forms dicoordinated complexes in the gas phase. Production of other gas-phase cluster ions such as $M^+(NH_3)_n$, $M^+(PH_3)_n$, $M^+(CO)_n$, etc., should also be possible, greatly expanding the current scope of quantitative gas-phase organometallic chemistry.

Acknowledgment. We thank William Wilcox at the University of Utah machine shop for considerable help in the construction of the SIMS-TQ instrument. We thank Professor J. H. Futrell for many helpful discussions. This work was supported by the National Science Foundation (Grant CHE 8796257).

(40) Caprioli, R. M. *Anal. Chem.* **1983**, *55*, 2387.